Femtosecond diffractive imaging of biological cells

Marvin M Seibert, Sébastien Boutet, Martin Svenda, Tomas Ekeberg, Filipe R N C Maia, Michael J Bogan, Nicusor Timneanu, Anton Barty, Stefan Hau-Riege, Carl Caleman, et al.

Femtosecond diffractive imaging of biological cells

Marvin M. Seibert[1], Sébastien Boutet[2,3,1], Martin Svenda[1], Tomas Ekeberg[1], Filipe R.N.C. Maia[1], Michael J. Bogan[2,3], Nicusor Tımneanu[1], Anton Barty[4,3], Stefan Hau-Riege[3], Carl Caleman[1], Matthias Frank[3], Henry Benner[3], Joanna Y. Lee[5], Stefano Marchesini[6], Joshua W. Shaevitz[7], Daniel A. Fletcher[8], Sasa Bajt[9], Inger Andersson[10], Henry N. Chapman[4] and Janos Hajdu[1]

[1] Laboratory of Molecular Biophysics, Department of Cell and Molecular Biology, Uppsala University, Husargatan 3, Box 596, SE-75124 Uppsala, Sweden
[2] SLAC National Accelerator Laboratory, 2575 Sand Hill Road, Menlo Park, California 94025, USA
[3] Lawrence Livermore National Laboratory, 7000 East Avenue, Livermore, California 94550, USA
[4] Center for Free-Electron Laser Science, University of Hamburg and DESY, Notkestrasse 85, Hamburg, Germany
[5] Department of Biology, Stanford University, Stanford, CA 94305, USA
[6] Advanced Light Source, Lawrence Berkeley National Laboratory, Berkeley, California 94720, USA
[7] Princeton University, 150 Carl Icahn Laboratory, Princeton NJ 08544, USA
[8] Bioengineering and Biophysics, University of California, Berkeley, California 94720, USA.
[9] Photon Science, DESY, Notkestrasse 85, 22607 Hamburg, Germany
[10] Swedish University of Agricultural Sciences, Department of Molecular Biology, Husargatan 3, Box 590, SE-751 24 Uppsala, Sweden

E-mail: **marvin.seibert@xray.bmc.uu**, **janos.hajdu@xray.bmc.uu.se**

Abbreviations
CXDI: coherent X-ray diffractive imaging, ESI: electrospray ionization, FEL: free-electron laser, FLASH: Free-electron Laser in Hamburg, LCLS: Linac Coherent Light Source, PRTF: phase retrieval transfer function, SEM: Scanning Electron Microscopy

Keywords
flash diffractive imaging, free-electron laser, *Prochlorococcus marinus*, *Spiroplasma melliferum*, *Synechococcus elongatus*, FLASH, soft X-ray laser

Abstract
In a flash diffraction experiment, a short and extremely intense X-ray pulse illuminates the sample to obtain a diffraction pattern before the onset of significant radiation damage. The over-sampled diffraction pattern permits phase retrieval through iterative phasing methods. Flash diffractive imaging was first demonstrated on an inorganic test object (Chapman et al. Nature Physics 2, 839-843, 2006). We report here experiments on biological systems where individual cells were imaged, using single, 10-15 femtoseconds soft X-ray pulses at 13.5 nm wavelength from the FLASH free-electron laser in Hamburg. Simulations show the pulse heated the sample to about 160,000 K but not before an interpretable diffraction pattern could be obtained. The reconstructed projection images return the structures of the intact cells. The simulations suggest the average displacement of ions and atoms in the hottest surface layers remained below 3 Å during the pulse.

Introduction

Coherent X-ray diffractive imaging (CXDI) is a technique in which an object is illuminated by a coherent beam of X-rays and the exit wavefront is reconstructed from the measurement of the amplitudes of the diffraction pattern. CXDI has been demonstrated with a variety of samples, ranging from simple test objects [1, 2], to crystals [3, 4] and cells [5-7]. Due to the considerable penetration depth of X-rays, CXDI permits studies on objects that would be too big for transmission electron microscopy.

A certain number of photons is required to impinge on the sample to achieve a desired resolution. High doses cause the very features of interest to be destroyed while low doses do not produce enough scattered signal to be measured. This is the dilemma of all structural sciences (for a review see [8]). There is a time component in all damage processes. At low dose rates, radiation damage has been shown to be dependent on the total dose on the sample [9]. It has been proposed that by greatly increasing the beam intensity and reducing the exposure time, a highly non-linear regime of dose-dependency could be reached, where a single diffraction pattern may be obtained at high resolution before damage has time to develop [10-13]. This requires pulses of duration shorter than the relevant dynamics involved in radiation damage. The first machines capable of producing such ultra-short brilliant pulses are free-electron lasers (FEL) [14-16]. The proof of principle of flash diffractive imaging was demonstrated on inorganic material at a wavelength of 32 nm at the VUV-FEL in Hamburg (renamed FLASH three weeks later), using a silicon nitride membrane with an etched pattern [17].

We report here use of this technique in biology for imaging individual biological cells. Three different single-celled organisms were imaged by flash diffraction, *Spiroplasma melliferum* [18, 19], *Prochlorococcus marinus* [20] and *Synechococcus elongatus* [21]. *S. elongatus* is a small photosynthetic cyanobacterium (1.5 μm x 0.8 μm) living in freshwaters. *P. marinus* is one of the smallest (c. 0.6 μm diameter) and most abundant species on Earth, distributed throughout the world's oceans between 40°N and 40°S. *Spiroplasmas* are pathogenic bacteria that lack cell walls and flagella; they infect plants, insects, and mammals [22, 23]. *Spiroplasmas*, including the species *S. melliferum* (5 μm x 0.15 μm), have a distinctive, easily identifiable extended helical morphology. *S. melliferum* has been shown to swim by a unique method of propagation of a pair of kinks along its length [18]. Those kinks are produced by a change in helical direction.

The three different samples chosen illustrate certain aspects of the developments needed in order to expand the capabilities of flash imaging for biological cells. *S. melliferum* is a particularly suitable sample, because its extreme thinness causes it to absorb little of the incoming beam at the wavelength used, making that the Born approximation valid. *P. marinus* represents a morphology that is more typical for single celled micro-organisms and extends this imaging method to micron-sized objects. The cluster of *S. elongatus* cells demonstrates the imaging and reconstruction of multiple isolated objects in a sparse image frame. The *S. elongatus* cells in direct contact can also serve as a substitute for illustrating the ability to image multi-cellular organisms, or several individual cells of one species simultaneously.

Results

Figure 1 shows the experimental arrangement. A 45^{o} graded multilayer mirror with a hole in its middle was used to let the direct beam pass through and reflect the scattered beam onto an upward facing charge-coupled device (CCD) detector. This experimental arrangement is described in detail in [17] and [24].

Figure 2 shows results from an imaging experiment on *Synechococcus elongatus* cells. Prior to the arrival of the pulse, the membrane, spanning the window held three *Synechococcus*

elongatus cells (Figure 2a), which were deposited from a 2 μl droplet of 25 mM ammonium acetate (pH 7.5) onto a 20 nm thick Si_3N_4 membrane. The top left of Figure 2b shows what happened to the sample-holding window after being hit by a single FLASH pulse (10 fs pulse length FWHM, 13.5 nm wavelength, focal diameter about 20-25 μm FWHM, 10^{14} W/cm^2). The membrane was completely destroyed (together with the cells), and parts of the surrounding silicon wafer were also ablated. The ablation crater in the bottom right-hand corner shows the effect of a similar FLASH pulse on the silicon wafer (covered with 20 nm thick silicon nitride layer) and gives an indication of the beam size and shape. Figure 2c shows that despite of the complete destruction of the cells, the image of the three cells can be retrieved from the diffraction pattern. No prior knowledge about the sample was used. The reconstructed image agrees with the microscopy image in Figure 2a. We note that it is practically impossible to make truly quantitative comparisons between reconstructed images from flash diffraction patterns and prior reference photographs taken by electron- or optical microscopy. The interactions are different, the sensitivities are different, and the response functions are different. Considering the resolutions available to us here, we judge agreements qualitatively by comparing (i) the shape, (ii) dimensions, and (iii) relative positions of particles in the reconstructions and the reference photographs.

A single-shot diffraction pattern of an individual *Prochloroccocus marinus* cell (Figure 3a) can be seen in Figure 3b. The cell was deposited directly onto a Si_3N_4 membrane by charge-reducing nano-electrospray ionization [see Methods]. This procedure made it possible for the cells to be isolated from their medium and to be electrostatically drawn to the membrane without contaminants (Figure 3b). The reconstructed exit wavefront is shown in Figure 3c. The diffraction pattern, re-calculated from the reconstructed image (Figure 3d), is in agreement with the experimentally recorded pattern (Figure 3b), supporting the accuracy of the reconstruction. The reconstructed exit wavefront was obtained by iterative phase retrieval in the HAWK software package [25]. The achieved resolution of the image was estimated by calculating the phase retrieval transfer function (PRTF) from 30 reconstructions. The PRTF falls below 1/e at 83nm resolution in this case (Figure 3e).

Figure 4 shows imaging results with the extremely thin *Spiroplasma* cells (150 nm diameter). These cells were deposited onto a poly-lysine coated silicon nitride window [see Methods]. This coating was uneven and contained randomly distributed clumps of material, as can be seen on Figure 4a. As a result, the background in the diffraction pattern (Figure 4b) was high. The small fringe spacings in the pattern correspond to spatial frequencies of 100 to 150 nm, which is the thickness of the cell. The reconstructed exit wavefront was obtained by iterative phase retrieval with the Shrinkwrap algorithm [26] [see Methods] and is shown in Figure 4c. This reconstruction agrees well with the electron micrograph of Figure 4a (taken prior to the exposure), and shows the helical shape of the cell accurately. The edge of the Si_3N_4 membrane (directly below the cell) is also reconstructed along with lumps of material on the membrane. Each pixel in the reconstruction corresponds to a size of 28 nm. The cell is about 0.15 μm thick and it is about 5 μm long. Only the large coherence length of the FLASH FEL beam makes it feasible to image such a large cell. The outstanding coherence properties of FLASH were exploited in an earlier experiment to image *S. melliferum* by massively parallel X-ray holography [27]. This gave a resolution of 75 nm. Our present results (Figure 4d) show significantly higher resolution (38 nm) than this earlier work. This is probably due to higher pulse intensities and to the fact that the coherence requirements of holography are significantly more stringent than for simple diffractive imaging. The PRTF for the present *S. melliferum* data (Figure 4d) was calculated from the 9 best reconstructions. The reconstructions selected had the closest agreement between the reconstructed diffracted amplitudes and the measured ones, using the lowest $\chi^2=\Sigma(A_r-A_m)^2/\ \Sigma(A_m)^2$, where A_r is the scattered amplitude of the reconstruction, A_m is the measured scattered amplitude and the sum

is over the entire array of pixels. The χ^2 value of the best fit was 2.3×10^{-4}. Due to the large amount of missing data from the central part of the pattern and the noise from the supporting membrane, multiple solutions were obtained and only the reconstructions that represented the same solution were averaged together. The retrieved phases can be seen to become less than 50% reproducible at a resolution of 45nm, or about three quarters of the way to the edge of the detector. If the point where the PRTF falls below 1/e is used to quantify the resolution, we get a resolution of 38 nm.

Simulations on sample heating (Figure 5a) and ion movement (Figure 5b) were performed according to [28] with the CRETIN software package [29] [see Methods]. The results show the FEL pulse heated the surface of the cells to about 160,000 K but none of the reconstructed projection images show measurable damage. Due to the high absorption cross section at 13.5 nm, the heating of the sample is not homogeneous. The average atomic displacement at the sample surface during illumination is in the sub-nanometer range (Figure 5b) and thus below the diffraction limited resolution.

Discussion

Recent measurements and simulations have shown little to no damage occurring in inorganic samples during pulses of 25 fs (FWHM) containing 10^{12} photons at 32 nm wavelength, and focused to a spot of 20-30 μm (FWHM) [13, 17, 30]. The results presented here demonstrate the feasibility of imaging micron-sized biological objects by flash diffraction. The FLASH facility at DESY in Hamburg is the first FEL operated as a user-facility [31]. The experiments described here used pulses of 25±20 μJ energy with a duration of 10-15 fs at a wavelength of 13.5 nm [16]. The large variation in the intensity of individual pulses, ranging from about 3×10^{11} photons to 3×10^{12} photons per pulse, arises from the stochastic nature of the lasing process [31]. The coherent beam, with an average of about 1.6×10^{12} photons/pulse, was focused to a spot of 20±5 μm FWHM diameter at the sample.

The problem with imaging large biological samples here is the lack of penetration power at 13.5 nm wavelength, the lack of contrast due to the very similar scattering cross section for the biologically relevant elements [32] and the difficulty of recording 3D patterns due to the irreproducibility of biological cells. The penetration power and resolution will continue to improve as FELs are upgraded and new sources are built with shorter wavelength. The Linac Coherent Light Source (LCLS) at Stanford is lasing at 1.5 Å wavelength. At longer wavelengths, high-harmonic sources driven by conventional lasers have recently reached sufficient brilliance for single-shot flash imaging [33]. The lack of contrast can be solved by taking advantage of large cross section differences inside the water window between about 2.3-4.4 nm wavelength [34]. The last problem is sample irreproducibility. Flash diffraction imaging offers the unique possibility to observe a projection of an individual sample in a unique conformation, rather than automatically producing the average structure of numerous copies of the object. This may allow the observation of projections of rare states and fleeting processes that are manifest in a class of structures which are generally non-reproducible. For reproducible samples, a recent theoretical study quantifies the effects of sample heterogeneity on achievable resolution [35].

Resolution could be improved with more intense FEL pulses, and also by removing the supporting membrane, and illuminating cells free of a support. This can be done by aerosolizing the microorganisms using electrospray ionisation [36, 37] or other types of nebulizers. Droplets containing single cells have been injected as a focused beam of particles into vacuum using aerodynamic lenses [38] and made to intersect with the FEL beam [39, 40], yielding container-free delivery of cells. Transfer of cells into the FEL beam from solution can be very rapid and this raises the possibility that the cells could still be alive and hydrated when intersecting the beam.

Methods

Sample Preparation

Synechococcus elongatus (PCC 6301) cells were grown in freshwater based Bg11 media. Before the imaging experiments, the cells were centrifuged at 6000 g for 10 minutes and the pellet resuspended in sterile 25 mM ammonium acetate. Cells were deposited from a droplet of 25 mM ammonium acetate (pH 7.5) onto a 20 nm thick Si_3N_4 membrane, and left to settle. Excess buffer was removed with a microcapillary. The 20 nm thick Si_3N_4 membranes have a transmission of 83% at 13.5 nm wavelength.

Prochlorococcus marinus cells were cultivated in Pro99 medium, based on sterile filtered Sargasso Sea water. Before the imaging experiments, cells were centrifuged at 8500 g for 10 minutes and resuspended in 25 mM ammonium acetate (viability in this medium was validated for periods of several hours). From this solution, cells were aerosolized with a nano-electrospray ionization (ESI) apparatus (TSI model 3480) operated with gas flows of 1.5 l/min sterile-filtered and dehumidified compressed air and 0.25 l/min of CO_2 at about 2 psi and a voltage of 1.9 kV. The highly charged droplets were neutralized by passing through a bipolar charged gas created with a Po^{210} alpha-particle emitter. The aerosol flow was directed towards a nanometer aerosol sampler (TSI model 3089) and captured on a silicon nitride membrane placed on top of an electrode held at a potential of -10 kV.

Spiroplasma melliferum cells were attached to silicon nitride membranes coated with polylysine. A solution of 0.01% poly-L-lysine of molecular weight 70-150 kDa (Sigma) was floated over the membrane for 30 minutes and formed a monolayer of roughly 10 nm, with a transmission of 94% of the beam at 13.5 nm. 10 µl of a solution containing glutaraldehyde-fixed *S. melliferum* was pipetted onto a section of the wafer containing 50 x 50 µm membranes and air dried. The *S. melliferum* cell was imaged using an electron microscope prior to illumination by the FLASH pulse and is shown in Figure 4a.

FEL Measurements

The FEL beam with a wavelength of 13.5 nm was focused using an ellipsoidal mirror to a 20 - 30 µm FWHM spot at the sample. The ellipsoidal mirror was located 2 m upstream of the sample. The sample was mounted on translation stages allowing different parts of the wafer to be illuminated. Stray light from the beamline was removed with a 2 mm aperture placed 29 mm upstream of the sample. Details of the FLASH beamline are presented in detail by [31].

The scattered beam was reflected off a 45^o resonant multilayer mirror, as previously described by [17, 24]. The direct beam was allowed to pass through a 1.5 mm hole in the middle of the multilayer mirror, removing the need to place a beamstop in front of the detector. Such a beamstop would ablate due to the FEL beam and the emitted radiation would add noise to the signal. The mirror used had a reflectivity of 65% at 13.5 nm. The mirror acts as a bandpass filter which reduces noise from plasma glow and other sources of photons at wavelengths different from the reflection characteristics of the mirror. The scattered beam, after reflection off the mirror was detected using a PI-MTE direct detection back-illuminated CCD from Princeton Instruments. The detector contained 1340 x 1300 pixels of 20 x 20 µm. With a CCD quantum efficiency of 42%, a total of 27% of the scattered photons were measured. The mirror/CCD assembly, as well as the sample and the pinhole were all mounted in *vacuo* to minimize scattering of the beam.

The direct beam can pass through the experiment. This is valuable for shot-to-shot beam characterization or can even be used to provide beam to another experiment in a tandem arrangement.

Simulations of Radiation Damage

For estimates on radiation damage on cells subjected to intense and short soft X-rays, we used the approach from [28]. Simulation on X-ray interaction with biological material were performed using the software CRETIN [29], a multi-dimensional radiation transfer code using non-local thermodynamic equilibrium. CRETIN provides a complete and proper physical treatment of fundamental physical processes involving ions and electrons, ionizations, collisions, recombinations, inverse bremsstrahlung, continuum lowering and can also treat the hydrodynamic expansion of the sample. CRETIN calculates level populations and transmission rates and produces absorption, heating rates and conduction coefficients during the entire simulation. The composition of the sample was taken to be $H_{23}C_3NO_{10}S$ (with a density of 1 g/cm^3), which is the average composition of a wet living cell containing 70% overall water. The heating was modeled in one dimension, justified by the X-ray focal size being much larger than the sample. The sample depth was divided into 400 zones which exchange energy through radiation transport and electron thermal conduction. The time evolution of the sample was followed with a time step of 10 as. The FEL pulse was modeled by a top hat function with a total length of 15 fs. Previous studies have shown that pulse shape had little impact on the ionization rates in the sample [34].

Image Reconstruction

As a consequence of having a hole in the mirror, the central part of the diffraction pattern is lost. If the missing data corresponds to too many oscillations in the diffraction pattern, many modes are unconstrained [41]. It is therefore essential to minimize the size of the hole in the mirror (or detector) and recover as much of the low-resolution data as possible. This was achieved here, and no prior knowledge was used in this work to populate the missing data.

Due to the low signal to noise ratio of the diffraction pattern at high angles in the *S. melliferum* diffraction pattern, the image reconstruction was originally performed with only the central half of the data. The 1340 x 1300 pixel diffracted amplitude array was cropped and only the middle 670 x 650 pixels were used. The autocorrelation function of the object was calculated from the Fourier transform of the diffracted intensity. The presence of point-like impurities in the sample produced low-resolution copies of the *Spiroplasma* cell in the autocorrelation function, a hologram. From the hologram a rough outline of the cell was created and used as the initial support. The diffracted wave was retrieved by the relaxed averaged alternating reflections (RAAR) algorithm in combination with Shrinkwrap. The only constraint used in image space was the finite support. After every 70 iterations, a new support was calculated from the latest iterate. The image was first convolved and then every pixel above a threshold was used as the new support. The size of the convolution kernel was progressively reduced from 3 pixels to 0.7 pixels after 7000 iterations. From the solution, a tight support was created, only slightly larger than the object, by again thresholding the image. This tight support was then enlarged by a factor of 2 in each direction and the entire diffraction data, not just the central half, was used to perform 200 separate reconstructions starting from different random phases. The tightness of the support around the object and the high contrast of the image lead to rapid convergence to a solution. Having this tight support made it possible to let the object be complex-valued [42, 43]. The curvature of the Ewald sphere was corrected for in the reconstruction, but it is a minor effect. The best fit to the data was selected and is shown in Figure 3a.

For the *P. marinus* and the *S. elongatus* reconstruction, the relaxed averaged alternating reflections (RAAR) algorithm in combination with Shrinkwrap was used to retrieve the phases of the diffracted wave starting from the autocorrelation function. The only constraint used in image space was the finite support. After every 20 iterations, a new support

was calculated from the latest iterate, by blurring the real-space image and including the brightest pixels in the support so that the support gets a certain area. Both the amount of blur and the support area were progressively decreased during reconstruction. The blur radius started at 3 pixels and was progressively decreased to 0.7 pixels at 7000 iterations. The area started at 2500 pixels and decreased to 200 pixels at 10000 iterations. The reconstruction was repeated 30 times from different random starting phases. The resulting images were averaged together after appropriate alignment and the resulting picture is shown in Figure 3c. The lack of inversion symmetry in the diffraction pattern is expected simply due to the amount of absorption at the wavelength used. In the *P. marinus* reconstructions, the support obtained using the shrinkwrap algorithm was sufficiently tight that a reconstruction of a complex-valued object was possible. Because the maximum angle of the signal was relatively small and the amount of oversampling was always high, the effect of the Ewald curvature was deemed sufficiently small to be neglected in this reconstruction.

Acknowledgements

We are grateful to the scientific and technical staff of FLASH at DESY, Hamburg, in particular to R. Treusch, S. Dusterer and S. Toleikis. We also thank T. Möller, C. Bostedt and H. Thomas for use of their vacuum chamber for these studies. We thank R. Lee and A. Szoke for discussions. This work was supported by the following agencies: The Swedish Research Council; The Swedish Foundation for International Cooperation in Research and Higher Education; The Swedish Foundation for Strategic Research; The Sven and Lilly Lawski Foundation (fellowship to MMS); Natural Sciences and Engineering Research Council of Canada through a Postdoctoral Fellowship to MJB (MJB is currently supported through the PULSE Institute at the SLAC National Accelerator Laboratory by the U.S. Department of Energy, Office of Basic Energy Sciences);The DFG Cluster of Excellence at the Munich Centre for Advanced Photonics, The National Science Foundation Center for Biophotonics, University of California, Davis: The Advanced Light Source, Lawrence Berkeley Lab, under DOE contract; The European Union (TUIXS); parts of this work were performed under the auspices of the U.S. Department of Energy by Lawrence Livermore National Laboratory under Contract DE-AC52-07NA27344. Simulations were performed on UPPMAX resources under project p2009018. Access to FLASH is provided by the European Union contract RII3-CT-2004-506008 (IA-SFS).

References

1. Miao, J.W., et al., *Extending the methodology of X-ray crystallography to allow imaging of micrometre-sized non-crystalline specimens.* Nature, 1999. **400**(6742): p. 342-344.
2. Loh, N.D., et al., *Cryptotomography: reconstructing 3D Fourier intensities from randomly oriented single-shot diffraction patterns.* . submitted, 2010.
3. Robinson, I.K., et al., *Reconstruction of the shapes of gold nanocrystals using coherent x-ray diffraction.* Physical Review Letters, 2001. **8719**(19): p. 195505.
4. Pfeifer, M.A., et al., *Three-dimensional mapping of a deformation field inside a nanocrystal.* Nature, 2006. **442**(7098): p. 63-66.
5. Miao, J.W., et al., *Imaging whole Escherichia coli bacteria by using single-particle x-ray diffraction.* Proceedings of the National Academy of Sciences of the United States of America, 2003. **100**(1): p. 110-112.
6. Shapiro, D., et al., *Biological imaging by soft x-ray diffraction microscopy.* Proceedings of the National Academy of Sciences of the United States of America, 2005. **102**(43): p. 15343-15346.
7. Mancuso, A.P., et al., *Coherent imaging of biological samples with femtosecond pulses at the free-electron laser FLASH.* New Journal of Physics, 2010. **12**: p. 035003.
8. Marchesini, S., et al., *Coherent X-ray diffractive imaging: applications and limitations.* Optics Express, 2003. **11**(19): p. 2344-2353.
9. Garman, E.F. and S.M. McSweeney, *Progress in research into radiation damage in cryo-cooled macromolecular crystals.* Journal of Synchrotron Radiation, 2007. **14**: p. 1-3.
10. Neutze, R., et al., *Potential for biomolecular imaging with femtosecond X-ray pulses.* Nature, 2000. **406**(6797): p. 752-757.
11. Hau-Riege, S.P., R.A. London, and A. Szoke, *Dynamics of biological molecules irradiated by short x-ray pulses.* Physical Review E, 2004. **69**(5): p. 051906.
12. Hau-Riege, S.P., et al., *Subnanometer-scale measurements of the interaction of ultrafast soft X-ray free-electron-laser pulses with matter.* Physical Review Letters, 2007. **98**(14): p. 145502.
13. Hau-Riege, S.P., et al., *Sacrificial Tamper Slows Down Sample Explosion in FLASH Diffraction Experiments.* Physical Review Letters, 2010. **104**(6): p. -.
14. Saldin, E.L., E.A. Schneidmiller, and M.V. Yurkov, *The Physics of Free-Electron Lasers - an Introduction.* Physics Reports-Review Section of Physics Letters, 1995. **260**(4-5): p. 187-327.
15. Ayvazyan, V., et al., *First operation of a free-electron laser generating GW power radiation at 32 nm wavelength.* European Physical Journal D, 2006. **37**(2): p. 297-303.
16. Ackermann, W., et al., *Operation of a free-electron laser from the extreme ultraviolet to the water window.* Nature Photonics, 2007. **1**(6): p. 336-342.
17. Chapman, H.N., et al., *Femtosecond diffractive imaging with a soft-X-ray free-electron laser.* Nature Physics, 2006. **2**(12): p. 839-843.
18. Shaevitz, J.W., J.Y. Lee, and D.A. Fletcher, *Spiroplasma swim by a processive change in body helicity.* Cell, 2005. **122**(6): p. 941-945.
19. Kurner, J., A.S. Frangakis, and W. Baumeister, *Cryo-electron tomography reveals the cytoskeletal structure of Spiroplasma melliferum.* Science, 2005. **307**(5708): p. 436-8.
20. Chisholm, S.W., et al., *A Novel Free-Living Prochlorophyte Abundant in the Oceanic Euphotic Zone.* Nature, 1988. **334**(6180): p. 340-343.
21. Nägeli, C., *Gattungen einzelliger Algen - physiologisch und systematisch bearbeitet.* 1849, Zürich: Frierich Schulthess.

22. Whitcomb, R.F., *The genus Spiroplasma.* Annu Rev Microbiol, 1980. **34**: p. 677-709.
23. Lorenz, B., J. Schroeder, and U. Reischl, *First evidence of an endogenous Spiroplasma sp. infection in humans manifesting as unilateral cataract associated with anterior uveitis in a premature baby.* Graefes Arch Clin Exp Ophthalmol, 2002. **240**(5): p. 348-53.
24. Bajt, S., et al., *Camera for coherent diffractive imaging and holography with a soft-x-ray free-electron laser.* Applied Optics, 2008. **47**(10): p. 1673-1683.
25. Maia, F., et al., *Hawk: the image reconstruction package for coherent X-ray diffractive imaging.* submitted, 2010.
26. Marchesini, S., *A unified evaluation of iterative projection algorithms for phase retrieval.* Review of Scientific Instruments, 2007. **78**(1): p. 011301.
27. Marchesini, S., et al., *Massively parallel X-ray holography.* Nature Photonics, 2008. **2**(9): p. 560-563.
28. Bergh, M., et al., *Interaction of ultrashort x-ray pulses with B4C, SiC, and Si.* Physical Review E, 2008. **77**(2): p. 026404.
29. Scott, H.A., *Cretin - a radiative transfer capability for laboratory plasmas.* Journal of Quantitative Spectroscopy & Radiative Transfer, 2001. **71**(2-6): p. 689-701.
30. Chapman, H.N., et al., *Femtosecond time-delay X-ray holography.* Nature, 2007. **448**(7154): p. 676-679.
31. Tiedtke, K., et al., *The soft x-ray free-electron laser FLASH at DESY: beamlines, diagnostics and end-stations.* New Journal of Physics, 2009. **11**: p. 023029.
32. Henke, B.L., E.M. Gullikson, and J.C. Davis, *X-Ray Interactions - Photoabsorption, Scattering, Transmission and Reflection at E=50-30,000 Ev, Z=1-92 (Vol 54, Pg 181, 1993).* Atomic Data and Nuclear Data Tables, 1993. **55**(2): p. 349-349.
33. Ravasio, A., et al., *Single-Shot Diffractive Imaging with a Table-Top Femtosecond Soft X-Ray Laser-Harmonics Source.* Physical Review Letters, 2009. **103**(2): p. 028104.
34. Bergh, M., et al., *Feasibility of imaging living cells at subnanometer resolutions by ultrafast X-ray diffraction.* Quarterly Reviews of Biophysics, 2008. **41**(3-4): p. 181-204.
35. Maia, F.R.N.C., et al., *Structural variability and the incoherent addition of scattered intensities in single-particle diffraction.* Physical Review E, 2009. **80**(3): p. 031905.
36. Bothner, B. and G. Siuzdak, *Electrospray ionization of a whole virus: Analyzing mass, structure, and viability.* Chembiochem, 2004. **5**(3): p. 258-260.
37. Clarke, J.D. and S.N. Jayasinghe, *Bio-electrosprayed multicellular zebrafish embryos are viable and develop normally.* Biomed Mater, 2008. **3**(1): p. 011001.
38. Liu, P., et al., *Generating Particle Beams of Controlled Dimensions and Divergence .1. Theory of Particle Motion in Aerodynamic Lenses and Nozzle Expansions.* Aerosol Science and Technology, 1995. **22**(3): p. 293-313.
39. Bogan, M.J., et al., *Single particle X-ray diffractive imaging.* Nano Letters, 2008. **8**(1): p. 310-316.
40. Chapman, H.N., et al., *Coherent Imaging at FLASH.* J Phys Conf, 2009. **186**: p. 012051.
41. Thibault, P., et al., *Reconstruction of a yeast cell from X-ray diffraction data.* Acta Crystallographica Section A, 2006. **62**: p. 248-261.
42. Fienup, J.R., *Reconstruction of a Complex-Valued Object from the Modulus of Its Fourier-Transform Using a Support Constraint.* Journal of the Optical Society of America a-Optics Image Science and Vision, 1987. **4**(1): p. 118-123.
43. He, H., et al., *Experimental lensless soft-X-ray imaging using iterative algorithms: phasing diffuse scattering.* Acta Crystallographica Section A, 2003. **59**: p. 143-152.

Figures with captions

Figure 1.

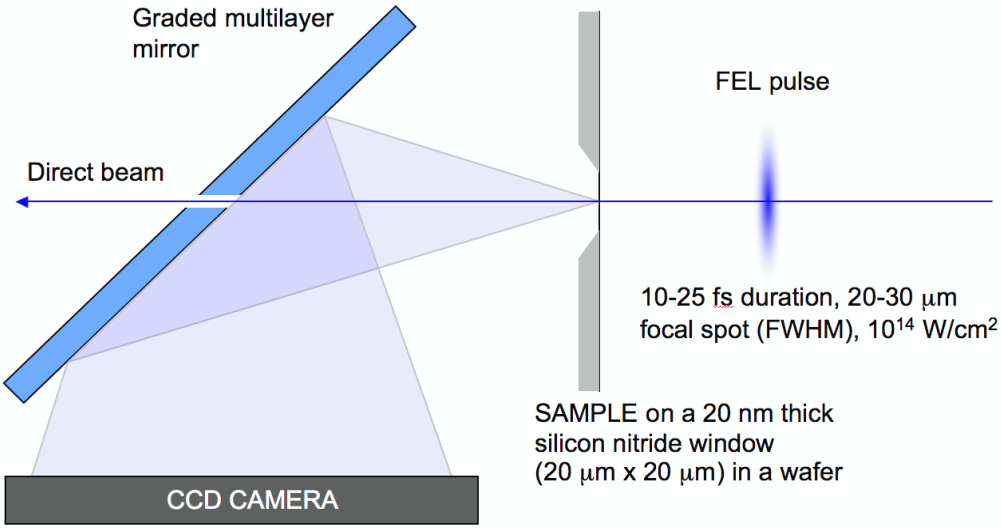

Figure 1. **The experimental setup.** The silicon-nitride sample window and the FEL pulse are significantly enlarged on the figure relative to the mirror and the CCD camera. The distance from the sample to the detector was 50 mm. The multilayer mirror has a hole in its centre to let the direct beam through. For details see refs [17, 24].

Figure 2.

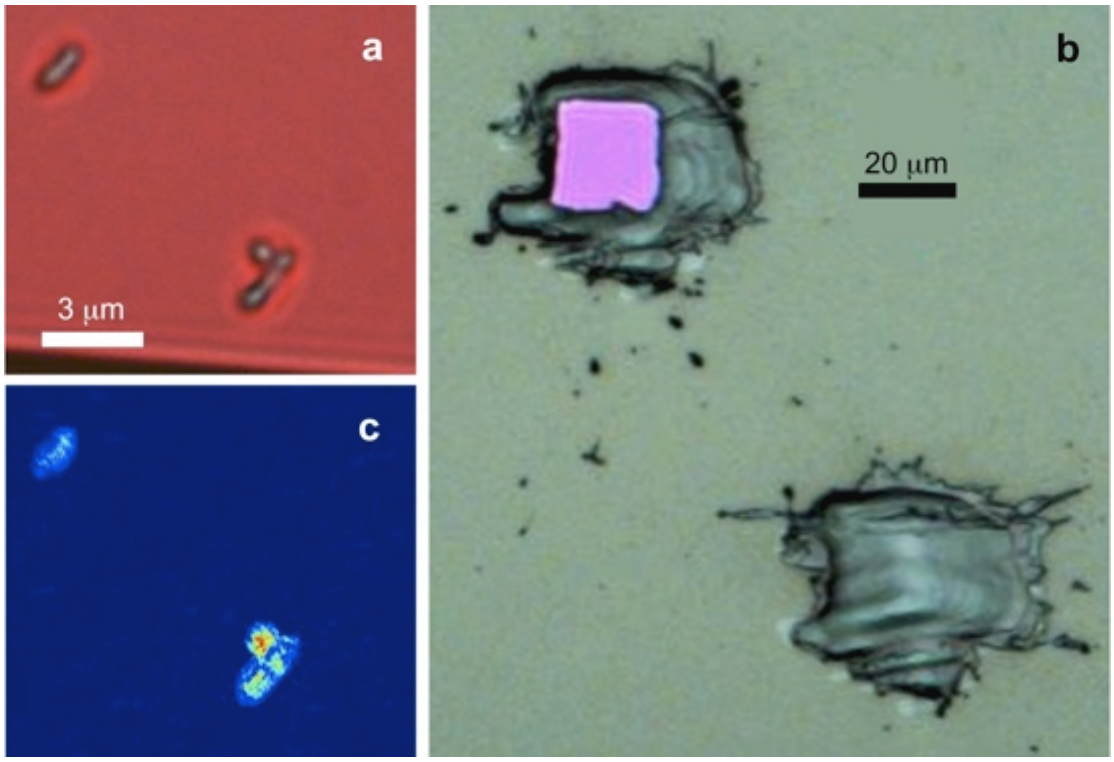

Figure 2. **Obliteration of *Synechococcus elongatus* cells by a single FLASH pulse**. (a) Photomicrograph of the intact cells on a silicon nitride window before exposure to the FLASH pulse. The edge of the window is visible at the bottom. (b) The same window (at a lower magnification) after being exposed to a c. 10 fs long FLASH pulse (FWHM) at 10^{14} W/cm^2, 13.5 nm wavelength. The wafer in the microscope was illuminated from two directions: with white light from above the sample plane and with a filtered "purple light" from below. This shows the blown out window as a purple square in (b). The crater at bottom right shows the profile of the FLASH beam from a similar shot. (c) The reconstructed exit wavefront from the diffraction pattern returns the image of the original cells.

Figure 3.

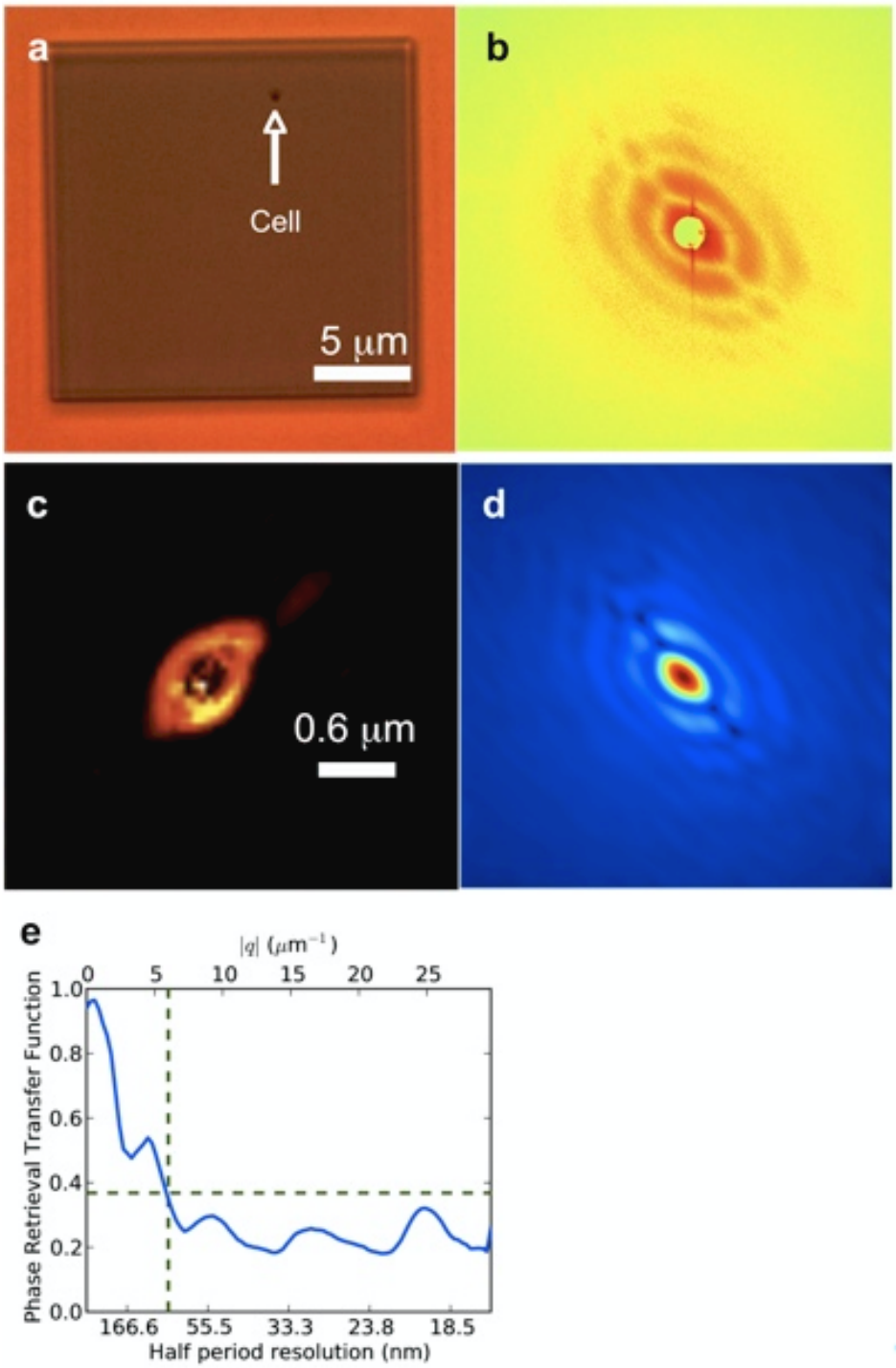

Figure 3. **Flash diffractive imaging of a *Prochlorococcoccus marinus* cell on a silicon nitride window.** (a) Light microscopy image of a single *P. marinus* on a 20 nm thick Si_3N_4 membrane. (b) The experimentally recorded diffraction pattern obtained with a FLASH pulse of approximately 10 fs (FWHM) at 13.5nm and displayed on a logarithmic scale. (c) The reconstructed exit wavefront obtained by iterative phase retrieval with the HAWK software package (Maia et al. 2010). (d) The diffraction pattern of *P. marinus*, computed from the reconstruction is in good agreement with the experimentally obtained pattern in (b). (e) The phase retrieval transfer function for the reconstructed *P. marinus* cell. The optical resolution is estimated to be 83 nm.

Figure 4.

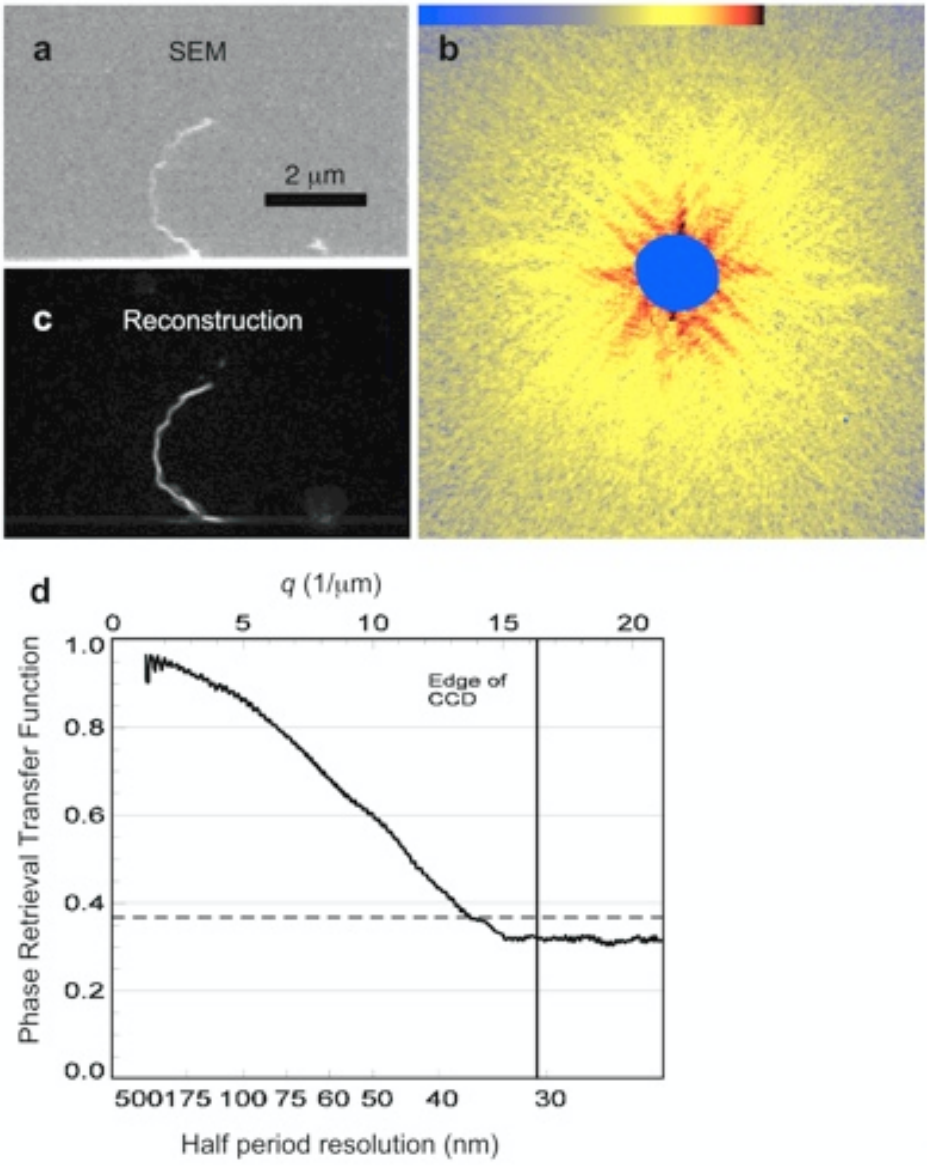

Figure 4. **Flash diffractive imaging of *Spiroplasma melliferum*.** (a) Scanning electron micrograph of a single glutaraldehyde-fixed *S. melliferum* cell on a Si_3N_4 membrane coated with a 10 nm thick layer of poly-L-lysine. (b) The diffraction pattern from this cell was obtained with a single FLASH pulse of 10-15 fs duration (FWHM) at 13.5 nm wavelength and 10^{14} W/cm^2. The shot destroyed the sample. The data are shown on a log scale after background subtraction with a range going from 0 (blue) to 58000 (black) photons per pixel. The diffraction pattern is noisy at high angles due to scattering from the poly-lysine coating on the membrane. (c) The modulus of the reconstructed exit wave is shown on a linear scale (see also [40]). Everything illuminated by the beam scatters and some 'dirt' spots are also reconstructed. The reconstruction shows excellent agreement with the electron micrograph in (a). (d) The phase retrieval transfer function was calculated from 9 different reconstructions that best matched the measured diffracted amplitudes of *S. melliferum*. The edge of the CCD corresponds to a resolution of 31 nm.

Figure 5.

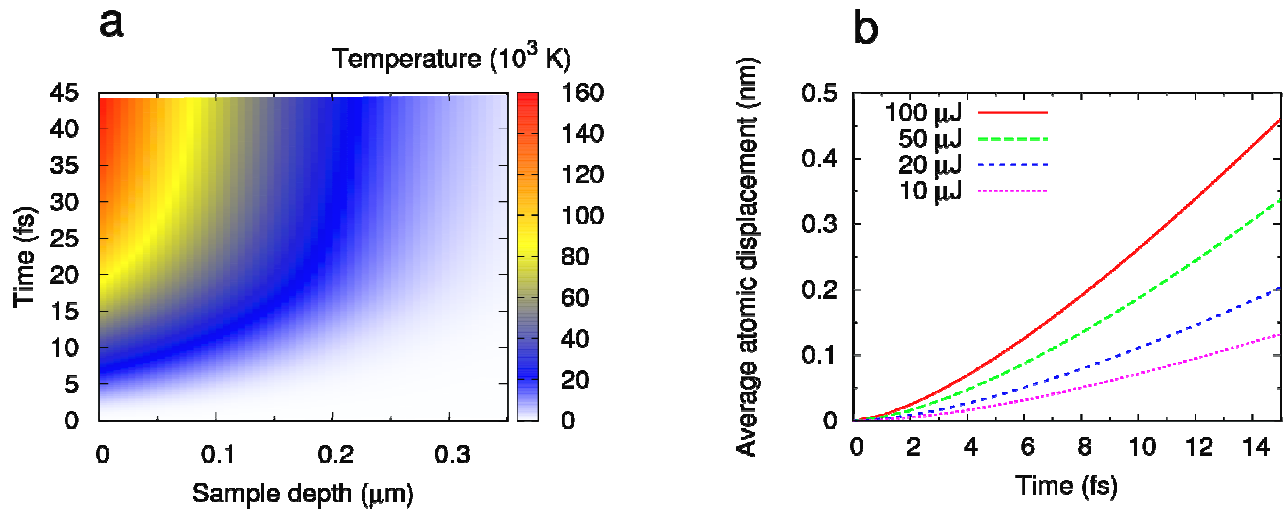

Figure 5. **Sample heating and radiation-induced sample movement during and after exposure to the FEL pulse.** (a) Ion temperature in the *P. marinus* sample during and after a 15 fs pulse as a function of sample depth. The pulse shape was modeled as a simple top-hat function. Pulse length = 15 fs, wavelength = 13.5 nm, pulse intensity = 20 μJ, focal spot = 20 μm. The sample becomes hottest on the side facing the X-ray beam. (b) Average displacement of ions and atoms on the illuminated surface during the pulse (15 fs) for several pulse intensities. The results show that the resolutions achieved in Figures 2-4 are not limited by atomic displacement or hydrodynamic expansion during the 15 fs long exposure.